Planar Dual-Band Baluns with Large Frequency Ratios and Improved Performance

Nguyen Manh HUNG [1], *Huynh Minh THUAN* [2], *Nguyen Minh GIANG* [2,*]

[1] Faculty of Electrical and Electronic Engineering, Hanoi Open University, 100000 Hanoi, Vietnam
[2] Faculty of Radio-electronic Engineering, Le Quy Don Technical University, 100000 Hanoi, Vietnam

giangnm@lqdtu.edu.vn

Submitted May 24, 2025 / Accepted December 5, 2025 / Online first January 20, 2026

Abstract. *In this paper, a novel design method for dual-band baluns operating with a high frequency ratio between the two bands is presented. The circuit is designed based on a dual-band cross-shaped impedance transformation circuit combined with a dual-band Pi-shaped phase shifter. The investigation results show that the proposed balun structure achieves a frequency ratio f_2/f_1 of up to 4.9, which exceeds the typical limits reported for most previously published dual-band balun circuits. The enhanced frequency ratio between the two bands enables the circuit to be applicable in wideband applications. To evaluate the effectiveness of the proposed design method, a prototype of dual-band balun operating at two bands f_1 = 0.7 GHz and f_2 = 2.3 GHz was designed, fabricated and measured. The measured results demonstrate that the proposed dual-band balun not only achieves a significantly large frequency ratio between the two bands but also ensures good performance in key parameters, particularly exhibiting a substantial improvement in amplitude imbalances. At the operating frequencies, the balun exhibits an insertion loss of less than 0.9 dB, isolation better than 23.4 dB, amplitude imbalance less than 0.19 dB, and phase difference of 180 ± 4.4 degrees.*

Keywords

Balun, dual-band, Pi-shaped, cross-shaped, large frequency ratio

1. Introduction

Balun circuits are essential components in many RF systems, serving the function of converting unbalanced signals to balanced signals. It is widely used in push-pull power amplifiers, balanced mixers, and antenna feed networks. In recent years, increasing interest in multiband applications has encouraged considerable research into balun circuits capable of operating over multiple frequency bands, including dual-, tri-, and quad-band designs [1–7], with dual-band being the most widely explored. Numerous design methodologies for dual-band baluns with improved performance have been proposed. In [8], a dual-band microstrip balun with integrated bandpass filter functionality is proposed, utilizing codirectional split-ring resonators loaded with interdigital capacitors. A compact dual-band balun, utilizing tapped open-ended stubs for size reduction, is presented in [9]. Another approach to designing a compact dual-band balun is based on SIW technology, as presented in [10]. A dual-band balun with improved isolation is designed in [11] by introducing an isolation circuit between the output ports. In [12], a balun circuit featuring wide bandwidth and high selectivity is presented. The design employs a slotline multi-mode T-line loaded middle-shorted complementary split-ring resonator.

Notably, dual-band balun circuits with a high frequency ratio between two bands (f_2/f_1) have received growing research attention in recent years [13–15]. Enhancing the frequency ratio between two bands not only enables the circuit to support wideband applications, but also makes it suitable for emerging multi-standard and multi-band communication systems, where a single balun must operate efficiently over widely separated frequency bands. Work [13] presents a dual-band balun design with a flexible frequency ratio, implemented using a four-port structure where the fourth port is open-circuited. The balun circuit [13] can achieve a frequency ratio f_2/f_1 of up to 3.8. In [14], a combination of coupled lines and open stubs was employed to achieve a dual-band balun with a high frequency ratio. As a result, the balun in [14] is capable of achieving a frequency ratio of up to 4.2. In [15], a dual-band balun is designed based on a symmetrical four-port network with one short-circuited port, where the frequency ratio between the two bands can be flexibly tuned over a wide range.

In this paper, a novel dual-band balun structure is presented. The proposed circuit can achieve a frequency ratio f_2/f_1 greater than that of most previously reported designs, with a maximum value of up to 4.9. Moreover, the critical performance parameters of the circuit remain well-maintained, and the amplitude imbalance, which is one of the key parameters, shows a significant improvement. The balun features a planar structure that combines a cross-shaped dual-band impedance transformer [16] and a dual-band 180-degree phase shifter. To validate the effectiveness of the proposed design, a prototype dual-band balun operating at two bands 0.7 GHz and 2.3 GHz was designed, fabricated, and tested. The close agreement between the measured results

DOI: 10.13164/re.2026.0067

and theoretical predictions validates the feasible configuration of the proposed dual-band balun.

2. The Proposed Dual-band Balun Structure

The balun functions to convert an unbalanced input signal into two balanced output signals with equal amplitude and a 180° phase difference. Therefore, the balun circuit can be designed by cascading a Wilkinson power divider with a 180° phase shifting circuit. The proposed dual-band balun is shown in Fig. 1, consisting of a dual-band power divider integrated with a dual-band 180° phase shifter.

The dual-band power divider is designed based on the traditional Wilkinson structure, in which the λ/4 transmission line sections of the traditional Wilkinson power divider are replaced by equivalent dual-band cross-shaped structures [16] (Fig. 2). With this configuration, the power divider operates at two frequency bands. An isolation resistor R_S with a value of 100 Ω is employed to enhance the isolation between the two output ports.

The cross-shaped structure consists of two transmission line sections with equal electrical length and characteristic impedance Z_1 and θ, an open stub (Z_m, θ) and a short stub (Z_S, θ) arranged in a cross configuration. Parameters of the cross-shaped circuit are designed such that the entire structure is equivalent to a quarter-wavelength transmission line with a characteristic impedance of Z_T at two operating frequencies, namely f_1 and f_2. Applying transmission line

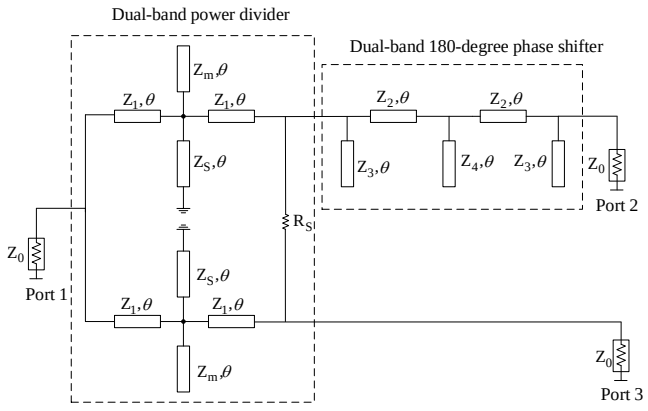

Fig. 1. Proposed dual-band balun with a large frequency ratio.

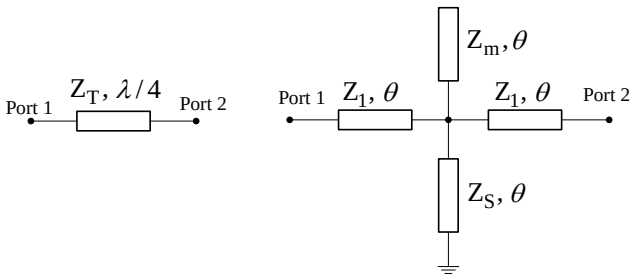

Fig. 2. A quarter-wavelength transmission line Z_T and its equivalent dual-band cross-shaped structure [16].

theory, the ABCD matrix of a cross-shaped structure $\mathbf{M}_{CS}$ is defined as follows

$$\mathbf{M}_{CS} = \mathbf{M}_1\mathbf{M}_s\mathbf{M}_m\mathbf{M}_1 \tag{1}$$

in which $\mathbf{M}_1$, $\mathbf{M}_S$, and $\mathbf{M}_m$, correspond to the ABCD matrices of transmission line (Z_1, θ), short stub (Z_S, θ), and open stub (Z_m, θ), respectively, and are defined as follows

$$\mathbf{M}_1 = \begin{bmatrix} \cos\theta & \mathrm{j}Z_1\sin\theta \\ \mathrm{j}Y_1\sin\theta & \cos\theta \end{bmatrix},\ \mathbf{M}_S = \begin{bmatrix} 1 & 0 \\ -\mathrm{j}/(Z_S\tan\theta) & 1 \end{bmatrix},$$

$$\mathbf{M}_m = \begin{bmatrix} 1 & 0 \\ \mathrm{j}Y_m\tan\theta & 1 \end{bmatrix}.$$

The ABCD matrix of a λ/4 transmission line section with a characteristic impedance Z_T is given by:

$$\mathbf{M}_T = \begin{bmatrix} 0 & \pm\mathrm{j}Z_T \\ \pm\mathrm{j}/Z_T & 0 \end{bmatrix}. \tag{2}$$

In order for the cross-shaped structure to be equivalent to the transmission line with characteristic impedance Z_T at frequencies f_1 and f_2, their ABCD matrices must be identical at these frequencies. In other words, (1) must be equivalent to (2). By solving this condition, the following relationships are obtained [16]:

$$Z_1 = \frac{Z_T}{\tan\theta}, \tag{3}$$

$$\frac{\tan\theta}{Z_m} - \frac{1}{Z_S\tan\theta} = \frac{\cos(2\theta)}{Z_T\cos^2\theta}. \tag{4}$$

The electrical length θ is determined based on the frequencies f_1 and f_2 as follows:

$$\theta = \frac{\pi}{1+\dfrac{f_2}{f_1}}. \tag{5}$$

Next, the dual-band 180° phase shifter is analyzed. It is implemented by cascading two dual-band 90° Pi-shaped phase shifters [17], as shown in Fig. 3.

Each dual-band Pi-shaped shifter is equivalent to a quarter-wavelength transmission line with a characteristic impedance Z_C at both frequency bands f_1 and f_2. According to [17], the parameters of the Pi-shaped circuit are calculated as follows

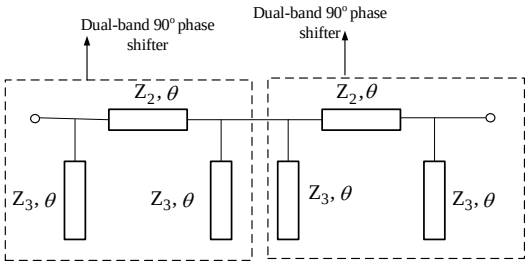

Fig. 3. A dual-band 180° phase shifter.

$$Z_2 = \frac{Z_C}{\sin\theta}, \tag{6}$$

$$Z_3 = Z_2 \tan^2\theta. \tag{7}$$

The electrical length θ is calculated by (5).

The phase shifter circuit in Fig. 3 consists of two shunt stubs (Z_3, θ); therefore, the circuit can be simplified by replacing them with a single equivalent shunt stub having the same electrical length θ and a characteristic impedance Z_4, which is determined as follows

$$Z_4 = \frac{Z_3 Z_3}{Z_3 + Z_3} = \frac{Z_3}{2}. \tag{8}$$

Thus, the simplified dual-band 180-degree phase shifter is shown in Fig. 4.

The dual-band 180-degree phase shifter is connected to one branch (the upper branch) of the dual-band power divider to form the dual-band balun presented in Fig. 1.

Next, the frequency ratio limit of the proposed dual-band balun will be investigated. The circuit can be fabricated on a microstrip structure using standard PCB technology if characteristic impedances of its transmission lines fall within 20 Ω to 120 Ω. This range ensures that the line widths remain practical for manufacturing, avoiding excessively wide lines that consume too much space and very narrow lines that are difficult to fabricate and prone to higher losses.

Based on (3)–(8), Figure 5 is constructed to show the variations of all characteristic impedances of the balun circuit, including Z_S, Z_1, Z_2, Z_3, and Z_4, as functions of the frequency ratio $n = f_2/f_1$, with Z_m chosen to be 25 Ω. From Fig. 5, it can be observed that in order to ensure all characteristic impedances of the balun circuit remain within the range of 20 Ω to 120 Ω, the allowable frequency ratio of the balun circuit must satisfy $2.8 \le f_2/f_1 \le 4.9$. It should be noted that although the impedance Z_4 becomes lower than 20 Ω at the frequency ratio $f_2/f_1 = 4.9$, this limitation can be effectively addressed by replacing Z_4 with two open stubs of characteristic impedance Z_3 (Fig. 3), connected in parallel. In this configuration, setting $Z_3 = 2Z_4$ maintains the equivalent conversion and ensures $Z_3 > 20$ Ω. As a result, the proposed dual-band balun remains feasible for a frequency ratio of 4.9, with all impedances staying within practical limits.

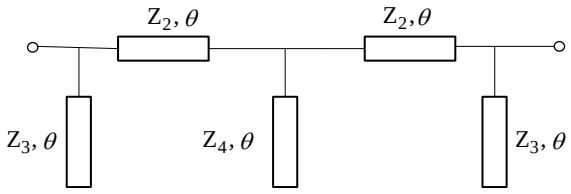

Fig. 4. A simplified dual-band 180° phase shifter.

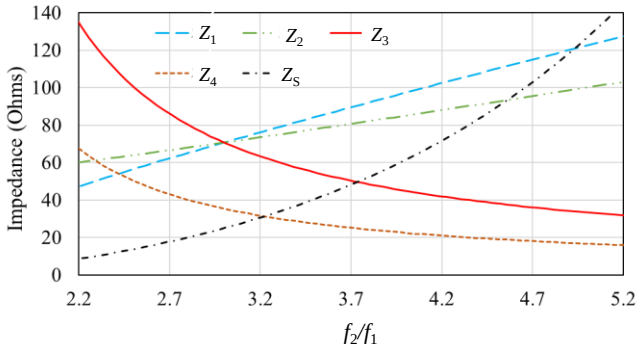

Fig. 5. Dependence of all characteristic impedances of the proposed dual-band balun on the frequency ratio f_2/f_1 with $Z_m = 25$ Ω.

It has been found that the allowable frequency ratio range of the proposed balun is significantly affected by the chosen value of Z_m. By applying the same analytical approach, the permissible frequency ratio f_2/f_1 can be determined for different values of Z_m. Table 1 summarizes the frequency ratio limits of the proposed dual-band balun for Z_m values ranging from 20 Ω to 120 Ω.

As can be seen from Tab. 1, the maximum achievable frequency ratio f_2/f_1 generally decreases with increasing Z_m. Specifically, when $Z_m \le 25$ Ω, the proposed dual-band balun achieves a frequency ratio of 4.9, which surpasses those reported in most previously published dual-band balun designs.

Next, Figure 6 presents the ideal simulated dependence of the bandwidths f_1 and f_2 on the frequency ratio f_2/f_1.The bandwidths are defined based on the condition that the amplitude imbalance is less than 0.5 dB. From Fig. 6(a), we can see that the bandwidth around f_1 increases as the frequency ratio f_2/f_1 becomes larger. This trend is consistent for all examined values of Z_m. Moreover, higher values of Z_m lead to wider bandwidths at f_1. This indicates that increasing Z_m is beneficial for enhancing the bandwidth at the lower frequency.

Meanwhile, Figure 6(b) indicates that while the bandwidth at f_2 decreases with increasing f_2/f_1, it remains adjustable via the choice of Z_m. Notably, larger Z_m values result in slightly enhanced bandwidths, emphasizing the tunability of the second band through proper impedance selection.

Figure 7 illustrates the dependence of the two phase-difference fractional bandwidths of the dual-band balun on the value of Z_m. The bandwidth is defined based on the criterion that the phase difference between the output ports remains within 180° ± 5°. As shown in Fig. 7, increasing the

Z_m (Ω)	f_2/f_1 range
20	3.0–4.9
25	2.8–4.9
30	2.66–4.51
40	2.49–4.0
60	2.32–3.49
80	2.24–3.24
100	2.19–3.1
120	2.16–3.0

Tab. 1. Variation of the allowable range of the frequency ratio f_2/f_1 versus characteristics impedance Z_m.

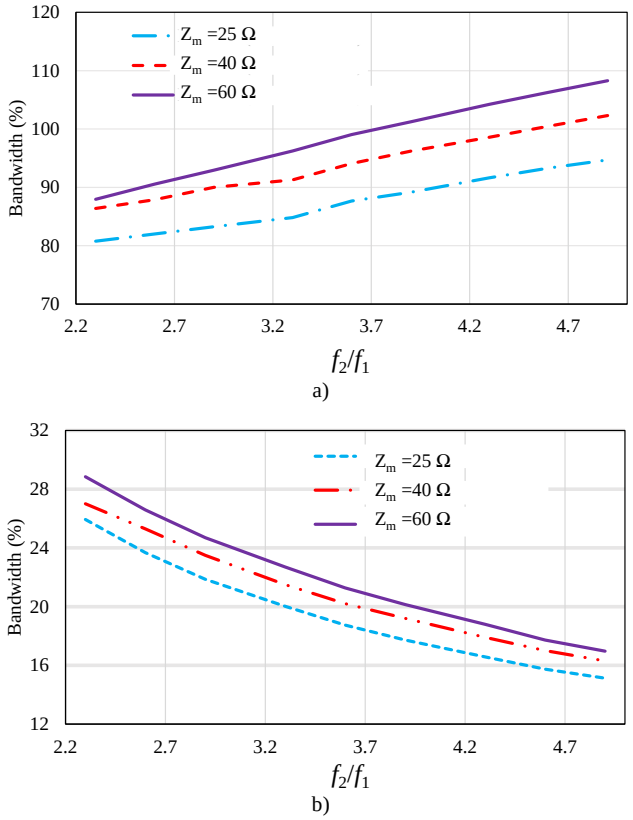

Fig. 6. The dependence of amplitude-imbalance bandwidth f_1 (a) and bandwidth f_2 (b) on the frequency ratio f_2/f_1 for different values of Z_m.

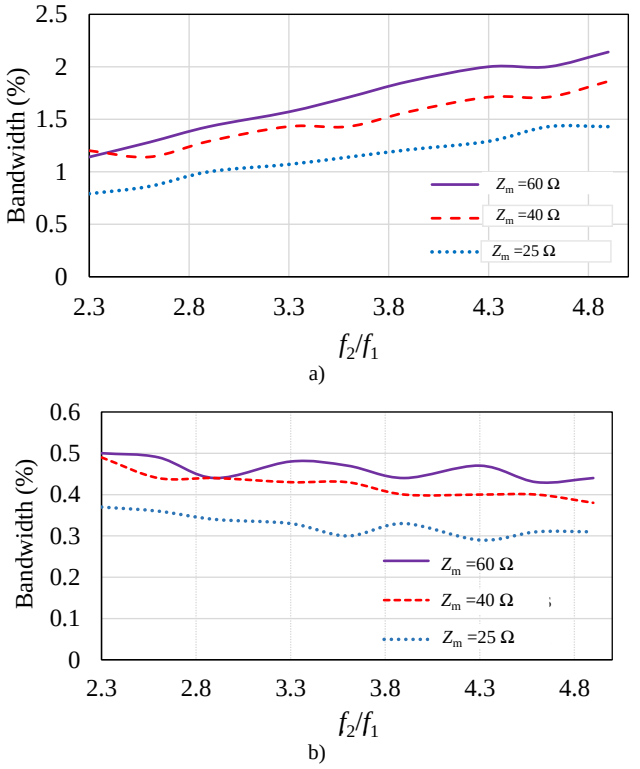

Fig. 7. The dependence of phase-difference bandwidth f_1 (a) and bandwidth f_2 (b) on the frequency ratio f_2/f_1 for different values of Z_m.

impedance Z_m leads to an increase in the bandwidths of both frequency bands that satisfy the phase-difference condition. Therefore, proper selection of Z_m, especially with larger values, provides an effective approach to enhancing the phase-difference bandwidth. Moreover, for a fixed Z_m, increasing the frequency ratio f_2/f_1 results in a wider bandwidth around f_1 but a narrower bandwidth around f_2. In contrast, decreasing the frequency ratio f_2/f_1 leads to a narrower bandwidth around f_1 and a wider bandwidth around f_2.

From the above analysis, it can be concluded that the proposed dual-band balun not only supports a large allowable frequency ratio but also provides the capability to control the bandwidths of the two operating bands through appropriate selection of the parameter Z_m. These are the remarkable features of the proposed circuit compared to previously reported dual-band baluns.

The design procedure for the dual-band balun circuit is summarized as follows:

Step 1: Select the two operating frequency bands, f_1 and f_2.

Step 2: Determine the electrical length θ using (5).

Step 3: From (3), calculate Z_1 with $Z_T = 70.71$ Ω.

Step 4: Based on the frequency ratio f_2/f_1 determined in step 1, Table 1 is used to select the appropriate value of Z_m. Then, Z_m and Z_1 are substituted into (4) to calculate Z_S.

Step 5: Calculate Z_2 using (6) with $Z_C = 50$ Ω. Then, determine Z_3 and Z_4 using (7), and (8), respectively.

3. Simulation and Experiment

To evaluate the proposed dual-band balun structure, this section presents the design, simulation, and fabrication of a prototype balun operating at two frequency bands: $f_1 = 0.7$ GHz and $f_2 = 2.3$ GHz. By applying the design procedure presented in the previous section, the design parameters of the circuit are determined as follows**.** From (5), the electrical length θ is calculated as $\theta = 42°$. Using (3), Z_1 is obtained as 78.5 Ω. Based on Tab. 1, impedance $Z_m = 40$ Ω is selected for the designed frequency ratio of $f_2/f_1 = 3.35$. Substituting the values of Z_m and Z_1 into (4), the resulting value of Z_S is 56 Ω. From (6), Z_2 is determined to be 74.72 Ω. Using (7) and (8), the values of Z_3 and Z_4 are 60.58 Ω and 30.29 Ω, respectively. The circuit is designed based on Rogers 4003C substrate with a thickness of 0.813 mm, a dielectric constant $\varepsilon_r = 3.55$, and a loss tangent of 0.0027.

The specific dimensions of designed balun are presented in Tab. 2.

Based on the calculated electrical lengths and characteristic impedances of all transmission line sections, in conjunction with the substrate parameters, the corresponding physical dimensions of each circuit section are calculated. The circuit was designed using Keysight ADS software. To account for layout effects and improve performance, the structure was further optimized using the built-in tuning and optimization tools of the software. The final optimized layout is shown in Fig. 8, and the corresponding physical di-

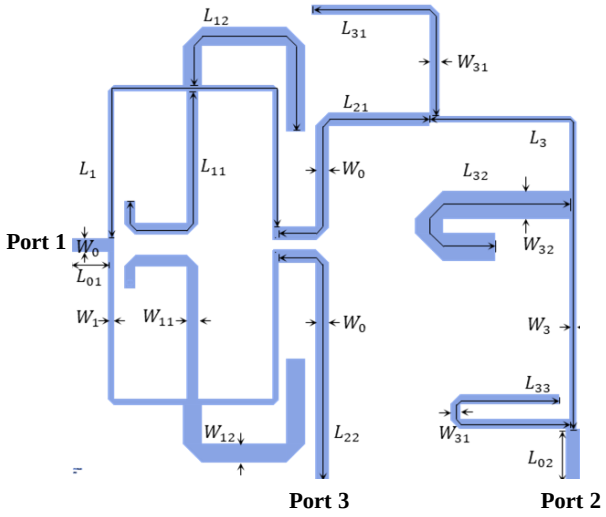

Fig. 8. Layout of the designed dual-band balun.

Dimension	Value (mm)	Dimension	Value (mm)
W_0	1.775	L_1	61.008
W_1	0.823	L_{11}	30.074
W_{11}	1.466	L_{12}	31.765
W_{12}	2.512	L_{21}	34.778
W_3	0.844	L_{22}	35.753
W_{31}	1.274	L_3	60.149
W_{32}	3.721	L_{31}	30.647
L_{01}	5	L_{32}	31.387
L_{02}	6.97	L_{33}	32.07

Tab. 2. Physical dimensions of transmission lines in the fabricated balun.

mensions are summarized in Tab. 2. The overall dimensions of the circuit are 65 mm × 75 mm.

After fabrication, the circuit is measured using a vector network analyzer. The fabricated circuit and measurement setup are illustrated in Fig. 9.

The measured and simulated results of the insertion loss parameters $|S_{21}|$ and $|S_{31}|$ of the dual-band balun are shown in Fig. 10. From Fig. 10, it can be observed that the measured results are in good agreement with the simulated ones. The center frequencies of the two operating bands obtained from the measurements are 0.68 GHz and 2.28 GHz,

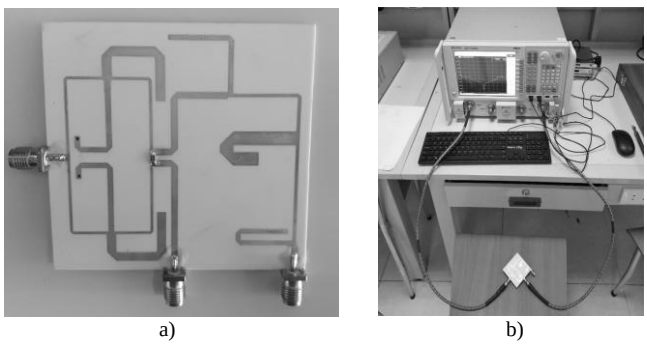

a) b)

Fig. 9. Photograph of the fabricated dual-band balun (a) and experimental setup (b).

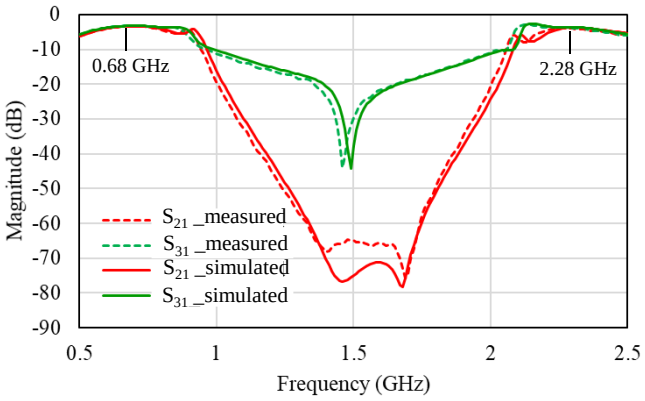

Fig. 10. Simulation and measurement of parameters S_{21} and S_{31} of the proposed dual-band balun.

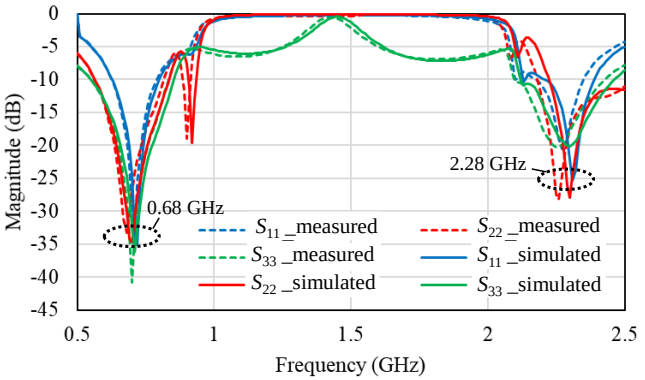

Fig. 11. Simulation and measurement of parameters S_{11}, S_{22}, and S_{33} of the proposed dual-band balun.

respectively. Compared to the theoretical values of 0.7 GHz and 2.3 GHz, the measured results show slight deviations. These small discrepancies are attributed to fabrication tolerances during the circuit manufacturing process. The measured insertion losses at the center frequency of 0.68 GHz are 3.3 dB and 3.2 dB for ports 2 ($|S_{21}|$) and 3 ($|S_{31}|$), respectively. Meanwhile, at 2.28 GHz, the values of $|S_{21}|$ and $|S_{31}|$ are 3.9 dB and 3.7 dB, respectively. Therefore, the measured insertion losses at both operating bands are consistent with the theoretical expectation of 3 dB, with a maximum deviation of no more than 0.9 dB.

Figure 11 illustrates both the simulated and measured return loss characteristics, given by the S-parameters $|S_{11}|$, $|S_{22}|$, and $|S_{33}|$, for the fabricated balun. At the center frequencies of 0.68 GHz and 2.28 GHz, all three parameters are observed to be below –19 dB, indicating good impedance matching at ports 1, 2, and 3.

Figure 12 shows the simulated and measured results of the isolation parameter $|\mathbf{S}_{23}|$ for the fabricated dual-band balun.

It is clear that the simulation and measurement curves are in good agreement. Two deep nulls in the magnitude of $|S_{23}|$ are observed at approximately 0.68 GHz and 2.28 GHz, corresponding to the center frequencies of the dual operating bands. At these frequencies, the measured values of $|S_{23}|$ are –26.2 dB and –23.4 dB, respectively, indicating excellent isolation between ports 2 and 3.

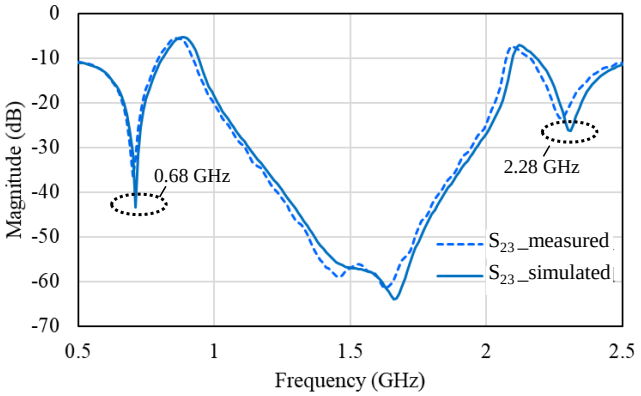

Fig. 12. Simulation and measurement of parameters S_{23} of the proposed dual-band balun.

Figure 13 shows the simulated and measured amplitude imbalance (AI) of the designed balun. The amplitude imbalance in decibels is defined as the absolute value of the difference between the magnitudes of S_{21} and S_{31}. Mathematically, this is written as:

$$\mathrm{AI(dB)} = \left|\left|S_{21}\right| - \left|S_{31}\right|\right|. \tag{9}$$

In (9), the terms $|S_{21}|$ and $|S_{31}|$ represent the magnitudes (in dB) of transmission coefficients S_{21} and S_{31}, respectively.

The amplitude imbalance is a key factor affecting the performance of balun circuits. It refers to the deviation in amplitude between the two differential output signals, which ideally should be equal. A large amplitude imbalance can lead to degraded signal integrity, reduced isolation, and increased distortion in balanced systems such as mixers, amplifiers, and antenna arrays. It can be observed from Fig. 13 that the measured amplitude imbalance (AI) approaches 0.096 dB dB and 0.19 dB at 0.68 GHz and 2.28 GHz, respectively. These values indicate excellent amplitude balance performance of the proposed dual-band balun at the targeted frequencies. Furthermore, the balun achieves a low amplitude imbalance of less than 0.5 dB over wide bandwidths, specifically 0.54–0.79 GHz (37.6%) for the first band and 2.23–2.5 GHz (11.4%) for the second band.

Figure 14 illustrates the measured and simulated phase difference (PD) of the fabricated balun. It is observed that the measured results are consistent with the simulations. Detailed data show that at the operating frequencies of 0.68 GHz and 2.28 GHz, the measured phase difference are 181.2° and 175.6°, respectively. Accordingly, the measured values deviate from the theoretical value of 180° by no more than 4.4°.

From the measured S-parameters, it can be observed that the fabricated dual-band balun achieves bandwidths of 0.65–0.74 GHz (12.9%) and 2.23–2.30 GHz (3.1%) for the first and second bands, respectively, under the condition of $|S_{11}| < -15$ dB. Within these operating bands, the magnitude imbalance is less than 0.43 dB, and the isolation is greater than 16.9 dB.

Finally, the measured scattering parameters of the fabricated dual-band balun are summarized in Tab. 3.

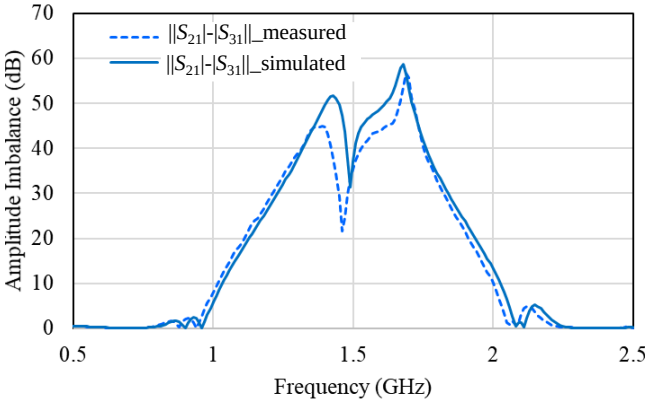

Fig. 13. Simulation and measurement AI of the proposed dual-band balun.

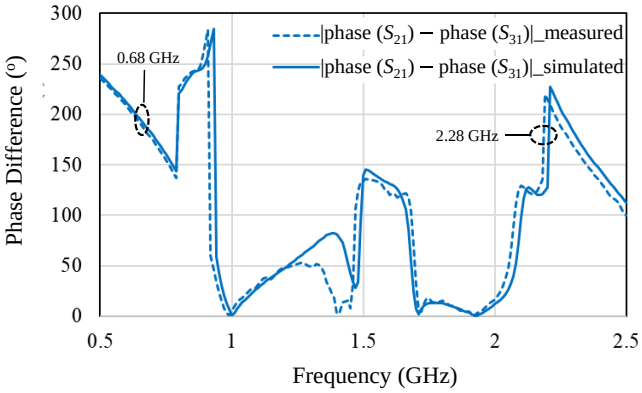

Fig. 14. Simulation and measurement PD of the proposed dual-band balun.

Frequency (GHz)	0.68	2.28
$\|S_{21}\|$ (dB)	−3.3	−3.9
$\|S_{31}\|$ (dB)	−3.2	−3.7
$\|S_{11}\|$ (dB)	−23.2	−19
$\|S_{22}\|$ (dB)	−33.3	−21.5
$\|S_{33}\|$ (dB)	−28.2	−19.4
$\|S_{23}\|$ (dB)	−26.2	−23.4
PD (°)	181.2	175.6
AI (dB)	0.096	0.193

Tab. 3. Measured scattering parameters of the fabricated dual-band balun.

Table 4 presents a comparison of the measured parameters of the fabricated dual-band balun with those of other works. In Tab. 4, IRL, IS, IL, and PD denote input return loss, isolation, insertion loss, and phase difference, respectively; MAFR–maximum allowable frequency ratio; NI–No information, λ_g is guided wavelength at frequency f_1.

As shown in Tab. 4, the proposed balun achieves a significantly large frequency ratio, with $f_2/f_1 = 3.353$, while its maximum allowable frequency ratio reaches 4.9. These values are notably higher than those reported in previous works, where f_2/f_1 typically ranges from 1.86 to 2.22, and the maximum allowable ratios remain below 4.6. In addition to its

Ref.	f_2/f_1	MAFR	IL (dB)	IRL (dB)	PD (deg)	AI (dB)	Structure	Size (λ^2_g)
[13]	1.86	3.8	< 0.75	NI	180 ± 1	NI	Using transmission lines, open stubs	NI
[14]	1.94	4.2	< 0.72	> 20.6	180 ± 1.4	NI	Based on pairs of coupled lines and open stubs	0.02
[15]	2.22	4.6	< 1.32	> 19	180 ± 2	< 0.34	Using coupled lines, transmission lines, and short stubs	0.04
[18]	2	3	NI	NI	180 ± 3	< 0.3	Based on stepped-impedance coupled line resonators	NI
[11]	2.13	NI	< 1.17	> 25	180 ± 1	NI	Using T-junction coupled lines, stepped-impedance stub lines	1.41
[19]	2.14	NI	< 1.3	> 19	180 ± 3.1	< 0.51	Using transmission line, open stubs	0.32
[9]	2.22	NI	< 1.53	NI	NI	NI	Based on coupled lines with short-ended port, and open stubs	NI
This work	**3.35**	**4.9**	**< 0.9**	**> 19**	**180 ± 4.4**	**< 0.19**	**Based on transmission lines, open and short stubs**	**0.089**

Tab. 4. Comparison between the measured performance of the proposed dual-band balun and other reported works.

superior frequency performance, the proposed balun also exhibits outstanding amplitude imbalance (AI), minimized to just 0.19 dB, which clearly outperforms all the designs listed in Tab. 4, where AI ranges from 0.3 to 0.51 dB. Furthermore, the design maintains a high return loss exceeding 19 dB, while its insertion loss remains below 0.9 dB, which is comparable to or better than those of most referenced designs.

With respect to physical size and structural complexity, the proposed dual-band balun exhibits certain advantages compared to previously reported designs. As shown in Tab. 4, the implemented circuit occupies an area of $0.089\ \lambda_g^2$, which is smaller than several prior works such as [11] ($1.41\ \lambda_g^2$) and [19] ($0.32\ \lambda_g^2$). Furthermore, the proposed structure employs a combination of transmission lines, open stubs, and short stubs, resulting in a relatively simple configuration that is easy to fabricate. This stands in contrast to other designs that rely on more complex structures such as stepped-impedance resonators [18], T-junctions coupled lines [11], or short-ended coupled-line sections [9]. Thus, the comparison results demonstrate that the proposed dual-band balun not only achieves a significantly large frequency ratio but also ensures good insertion and return losses, as well as minimal amplitude imbalance, making it highly suitable for broadband and multi-band microwave applications

4. Conclusions

In this work, a novel design for dual-band baluns with a high frequency ratio has been proposed and validated. The balun circuit is designed using a dual-band cross-shaped impedance transformer combined with a Pi-shaped phase shifter, enabling operation at widely separated frequency bands. The analysis results show that the proposed dual-band balun structure supports a frequency ratio of up to 4.9, exceeding the typical limitations of most previously reported dual-band baluns. Furthermore, the fabricated prototype, operating at 0.7 GHz and 2.3 GHz, demonstrates improved amplitude imbalance while still ensuring good insertion loss, isolation, and phase difference. These results indicate that the proposed balun structure is a promising solution for wideband and multi-band RF applications.

References

[1] BARIK, R. K., KUMAR, K. V. P., KARTHIKEYAN, S. S. Design of a quad-band branch line balun using extended Pi-shaped coupled lines. *IEEE Microwave and Wireless Components Letters*, 2016, vol. 26, no. 10, p. 771–773. DOI: 10.1109/LMWC.2016.2605438

[2] FENG, Z., BI, X. Quad-band balun filter using dual-mode spiral slotline notched structure with enhanced selectivity. In *2019 IEEE International Conference on Integrated Circuits, Technologies and Applications (ICTA)*. Chengdu (China), 2019, p. 164–165. DOI: 10.1109/ICTA48799.2019.9012909

[3] BARIK, R. K., CHENG, Q. S., KOZIEL, S. Design and experimental validation of highly compact branch-line balun for quad-band applications. In *2021 IEEE MTT-S International Wireless Symposium (IWS)*. Nanjing (China), 2021, p. 1–3. DOI: 10.1109/IWS52775.2021.9499527

[4] GUPTA, R., YADAV, A. P., HASHMI, M. S. Symmetric tri-band balun architecture with a systematic design procedure. In *2017 Twenty-third National Conference on Communications (NCC)*. Chennai (India), 2017, p. 1–5. DOI: 10.1109/NCC.2017.8077126

[5] LIOU, C. Y., MAO, S. G. Triple-band Marchand balun filter using coupled-line admittance inverter technique. *IEEE Transactions on Microwave Theory and Techniques*, 2013, vol. 61, no. 11, p. 3846 to 3852. DOI: 10.1109/TMTT.2013.2281177

[6] ZHANG, H., PENG, Y., XIN, H. A tapped stepped-impedance balun with dual-band operations. *IEEE Antennas and Wireless Propagation Letters*, 2008, vol. 7, p. 119–122. DOI: 10.1109/LAWP.2008.921315

[7] LI, Y. C., LI, L. W., WU, D.-S., et al. Dual-mode dual-band DR balun filter using suspended stripline feeding structure. *IEEE Microwave and Wireless Components Letters*, 2022, vol. 32, no. 6, p. 503–506. DOI: 10.1109/LMWC.2022.3142906

[8] GORUR, A. K. A dual-band balun BPF using codirectional split ring resonators. *IEEE Microwave and Wireless Components Letters*, 2020, vol. 30, no. 10, p. 949–952. DOI: 10.1109/LMWC.2020.3016622

[9] SHAO, J., ZHANG, H., CHEN, C., et al. A compact dual-band coupled-line balun with tapped open-ended stubs. *Progress In Electromagnetics Research C*, 2011, vol. 22, p. 109–122. DOI: 10.2528/PIERC11050205

[10] ZHU, F., WU, Y., CHU, P., et al. Compact dual-band filtering baluns using perturbed substrate integrated waveguide circular cavities. *IEEE Microwave and Wireless Technology Letters*, 2023, vol. 33, no. 6, p. 663–666. DOI: 10.1109/LMWT.2023.3243646

[11] LI, E. S., LIN, C.-T., JIN, H., et al. A systematic design method for a dual-band balun with impedance transformation and high isolation. *IEEE Access*, 2019, vol. 7, p. 143805–143813. DOI: 10.1109/ACCESS.2019.2945049

[12] ZENG, X., BI, X., CAO, Z., et al. High selectivity dual-wideband balun filter utilizing a multimode T-line loaded middle-shorted CSRR. *IEEE Transactions on Circuits and Systems II: Express Briefs*, 2020, vol. 67, no. 11, p. 2447–2451. DOI: 10.1109/TCSII.2020.2963907

[13] LI SHEN, A., ZHOU, M., ARIGONG, B., et al. Dual-band balun with flexible frequency ratios. *Electronics Letters*, 2014, vol. 51, no. 17, p. 1213–1214. DOI: 10.1049/el.2014.1110

[14] ZHANG, W., WU, Y., YU, C., et al. Planar compact dual-band balun with flexible frequency ratios. *Electromagnetics*, 2017, vol. 37, no. 1, p. 64–72. DOI: 10.1080/02726343.2017.1261313

[15] HUANG, F., WANG, J., ZHU, L., et al. Dual-band microstrip balun with flexible frequency ratio and high selectivity. *IEEE Microwave and Wireless Components Letters*, 2017, vol. 27, no. 11, p. 962–964. DOI: 10.1109/LMWC.2017.2750021

[16] ZHANG, H., XIN, H. Designs of dual-band Wilkinson power dividers with flexible frequency ratios. In *2008 IEEE MTT-S International Microwave Symposium Digest*. Atlanta (GA, USA), 2008, p. 1223–1226. DOI: 10.1109/MWSYM.2008.4633279

[17] KIM, T., LEE, B., PARK, M.-J. Dual-band unequal Wilkinson power divider with reduced length. *Microwave and Optical Technology Letters*, 2010, vol. 25, no. 5, p. 1187–1190. DOI: 10.1002/mop.25119

[18] GAO, X., YEUNG, L. K., WU, K.-L. A dual-band balun using partially coupled stepped-impedance coupled-line resonators. *IEEE Transactions on Microwave Theory and Techniques*, 2008, vol. 56, no. 6, p. 1455–1460. DOI: 10.1109/TMTT.2008.923338

[19] YOON YANG, S., SIK CHO, C., LEE, J. W., et al. A novel dual-band balun using branch-lines with open stubs. *Microwave and Optical Technology Letters*, 2007, vol. 49, no. 5, p. 1162–1164. DOI: 10.1002/mop.24996

About the Authors ...

Nguyen Manh HUNG received his B.S. degree in Electronics and Telecommunications from the Le Quy Don Technical University, Hanoi, Vietnam, in 2013. He received his M.S. degree in Telecommunications Engineering from the Posts and Telecommunications Institute of Technology in 2015. He is currently a lecturer at the Faculty of Electrical and Electronic Engineering, Hanoi Open University, Vietnam. His research interests include electronics, MIMO antennas, and IC programming.

Huynh Minh THUAN was born in Ca Mau, Vietnam. He received a Diploma in Telecommunications Engineering from Le Quy Don Technical University, expected to graduate in 2025. His research interests include RF design and microwave engineering.

Nguyen Minh GIANG (corresponding author) was born in Thai Nguyen, VietNam. He received the D.E. degree in Electronics Engineering from Irkutsk National State Technical University, Russia, in 2018. He is currently a Senior Lecturer at the Le Quy Don Technical University, Hanoi, Vietnam. His research interests include RF design and microwave engineering.